

# Multi-holed clay nanotubes and their modification with a polyaniline nanolayer

C. Zhou · X. Du · Z. Liu · Y.-W. Mai ·  
S. P. Ringer

Received: 5 July 2010/Accepted: 7 September 2010/Published online: 21 September 2010  
© Springer Science+Business Media, LLC 2010

**Abstract** A facile *in situ* mechanical–chemical polymerization method for synthesis of polyaniline/halloysite nanocomposites was developed. Electron micrographs of the composites showed novel multi-holed clay nanotubes modified with a porous polyaniline nanolayer. After removing clay tube cores, polyaniline nanotubes can be obtained. Moreover, novel multi-holed clay nanotubes were obtained after removing polymer shells.

## Introduction

Polyaniline (PANI) is one of the important conductive polymers, and many solution-based chemical methods to prepare nanostructured PANI and its nanocomposites have been developed [1–5]. As a simple and convenient chemical reaction method, mechanochemical reaction has been used to prepare various inorganic nanomaterials. Recently, this method has been extended successfully to prepare polymer and the composite materials [6–9].

Halloysite nanotubes has been studied for applications in many fields, such as adsorbents [10], fillers in nanocomposites [11], and substrates for catalysts [12] or nano-containers for biomolecules[13]. Here, we describe a simple route to modify halloysite with PANI via *in situ* mechanochemical polymerization of aniline in the presence of the clay nanotubes. Interestingly, we found that the

resultant composite showed a novel nanostructure comprising clay tubes with nanoholes on the sidewalls.

## Experimental

Polyaniline (PANI)/halloysite nanocomposite was prepared using the following procedure. In a typical process, 1 mL aniline and 0.6 g halloysite were mixed and hand-ground for 1 min, and 5 g FeCl<sub>3</sub> was then added and mixed together with further grinding. After grinding for another 40 min, the product was collected and purified by washing with water and filtration using a Buchner funnel with a water aspirator. A small portion of the wet product was then dispersed in ethanol for TEM studies on a Philips CM12. The other part of product was dried at 80 °C for 12 h. XRD were obtained on a Siemens 5000 X-ray diffractometer. SEM observations were performed on a Zeiss ULTRA-plus. FT-IR and UV-vis spectra were recorded on a Varian FT-IR and a Cary 5 UV-vis spectrometer, respectively. DSC data was obtained on TA DSC 2920. A CHI1202A Electrochemical Analyzer was used for electrochemical measurements. The pore size and volume of the samples were determined from nitrogen adsorption isotherms measured using a Quantachrome Autosorb 1 gas sorption system. The electrical conductivity data was measured on the pressed pellet of the samples with conventional 2 probe method. The pellets were obtained by pressing the powder at 20 MPa.

## Results and discussion

The FT-IR spectrum of halloysite (Fig. 1a) exhibits its characteristic bands at 3691 and 3620 cm<sup>-1</sup>, which can be

C. Zhou · Z. Liu · S. P. Ringer  
Australian Centre for Microscopy and Microanalysis,  
University of Sydney, Sydney, NSW 2006, Australia

X. Du (✉) · Y.-W. Mai  
School of Aerospace Mechanical Mechatronic Engineering J07,  
University of Sydney, Sydney, NSW 2006, Australia  
e-mail: xdu@usyd.edu.au

attributed to two  $\text{Al}_2\text{OH}$ -stretching bands with each OH linked to two Al atoms [14]. The two weak bands at 3546 and  $3480 \text{ cm}^{-1}$  can be attributed to the intercalated water and surface OH groups (H-bonded to interlayer water), respectively. The water bending band is also observed at  $1633 \text{ cm}^{-1}$ . There are a few characteristic bands of this mineral: 1117, 1011, and  $1005 \text{ cm}^{-1}$  (Si–O stretching modes),  $908 \text{ cm}^{-1}$  ( $\text{Al}_2\text{OH}$ ). In the magnified parts (see inset in Fig. 1) of the spectrum, the additional two weak bands at  $3646 \text{ cm}^{-1}$  and  $3672 \text{ cm}^{-1}$ , and the shoulder band at  $935 \text{ cm}^{-1}$  to the  $908 \text{ cm}^{-1}$ , indicate the presence of kaolin impurities [15], since generally halloysite shows only two bands and a single  $\text{Al}_2\text{OH}$ -bending band at  $\sim 908 \text{ cm}^{-1}$  but kaolinites exhibits four bands and a shoulder accompanying the  $\text{Al}_2\text{OH}$ -bending band in the corresponding range [14]. The presence of the hydroxyl groups could facilitate the adsorption of aniline monomer through H-bond and the restriction of the polymerization on the clay tube surfaces.

The FTIR spectra of PANi (Fig. 1c) show its characteristic absorption bands at 1573, 1486, 1296, and  $1242 \text{ cm}^{-1}$ , which can be attributed to the C=C stretching vibration mode of the quinonoid and benzenoid rings, the stretching mode of C–N and the protonated C–N group, respectively [8, 16]. It is noted that the intensity of the band at  $1573 \text{ cm}^{-1}$  relative to that at  $1486 \text{ cm}^{-1}$  increases in the spectrum of the composite (Fig. 1b), indicating the composite is richer in quinonoid units than PANi. The UV–vis spectrum of PANi without clay (Fig. 2) shows the characteristic absorption peaks of PANi in its emeraldine base (EB) state, where a narrow peak at 323 nm and broad peak at 620 nm appear, corresponding to the  $\pi-\pi^*$  transition centered on the benzenoid unit and to the quinonoid

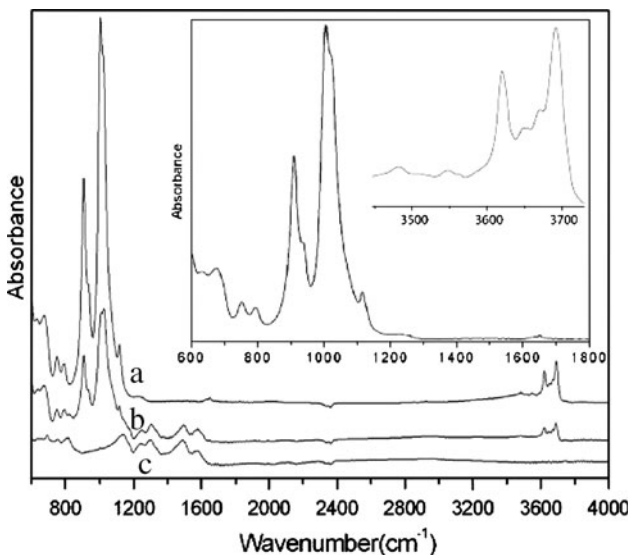


**Fig. 1** FTIR-ATR spectrum of (a) halloysites, (b) PANi/halloysite composite, and (c) PANi

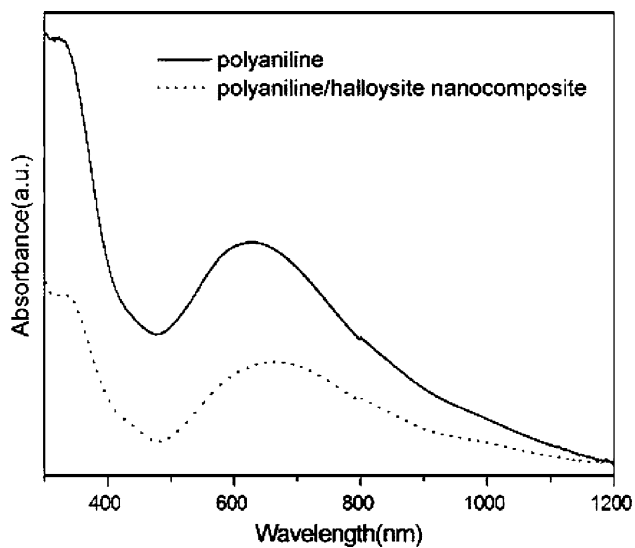


**Fig. 2** UV–vis spectra of PANi and PANi/halloysite nanocomposite

excitation band, respectively. While in the UV spectrum of the composite, both peaks shifted to higher wavelength, e.g., 332 and 663 nm, respectively. These shifts can come from the interaction between the polymer and the halloysites. This is in accordance with the red shifts observed for PPy-MMT clay [17] and PANi-Mica [18] by other groups. It is likely that the interfacial H-bonding interactions between aniline and clay restricts the polymerization on the halloysite tube surface and uncoil the PANi chain, leading to the increase of its conjugation length. This interaction therefore causes a red shift in the UV–vis absorption spectra. This is similar to the case that the intercalation of conjugated polymers inside clay galleries by an in situ polymerization of the trapped monomers induces the improvement of their conjugation degree due to the creation of more preferential orientations than the PANi molecules formed in a coiled state without the tube templates [18]. The polymerization occurring on the surface of the halloysite clay tubes may make the polymer chains more straightened resulting into a higher degree of conjugation and causing a red shift of the peaks in its UV–vis spectra.

In the XRD pattern of halloysite, the basal space reflections indicate a sharp peak at  $12.4^\circ$  corresponding to a 001 basal spacing of 0.72 nm. While in the one of PANi, only one broad peak around  $2\theta = 21^\circ$  can be observed, which is the typical amorphous scattering of PANi in its EB form [19]. The pattern of the composite is almost the same as that of halloysite, confirming the retaining of its structure. In the DSC curve of the halloysite, the first weak peak around  $115^\circ\text{C}$  can be attributed to the loss of adsorbed water, and the strong peak around  $590^\circ\text{C}$  is due to the de-hydroxyl groups, similar to previously reported DTA results [14]. Both peaks are shifted to higher temperatures in the curve of the composite, e.g., 150 and

610 °C, respectively. The shifts can be attributed to the coating effect of the polymer layer, probably from the H-bonding interaction between the H–N group in PANi and the hydroxyl group in the clay, as discussed above. The endothermic peak at 490 °C is caused by the decomposition of the PANi macromolecule [20]. As the content of PANi in the composite is only 18 wt% and the polymer is in its EB form, the conductivity of the composite ( $1.64 \times 10^{-6}$  S/cm) is less than those prepared in acid aqueous solutions [21]. The electrochemical characteristics of the composite were also investigated by cyclic voltammetry (Fig. 3), where the oxidation process with a peak at

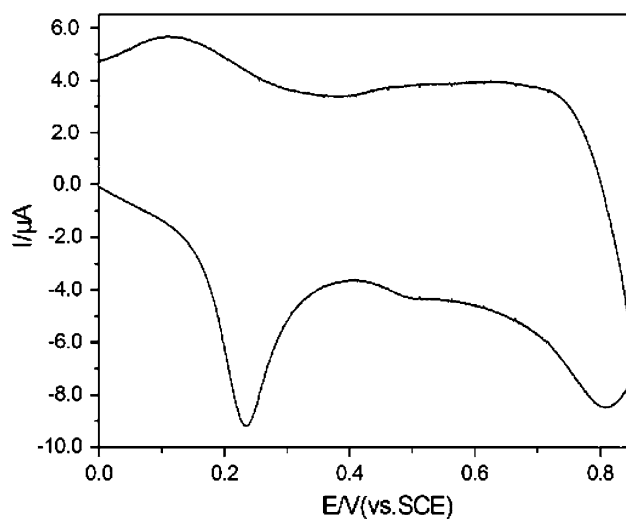


**Fig. 3** CV of PANi/halloysite composite in 1 M HCl aqueous solution with a scan rate of 0.5 V/s

~0.23 V is caused by the oxidation of the leucoemeraldine to the emeraldine form, and the peak at ~0.81 V is a result of the oxidation from the emeraldine to the pernigraniline form [22], indicating that the composite is electrochemically active.

Microscopic examinations of halloysites (Fig. 4a, b) reveal that the sample contains mainly nanotubes with lengths up to  $\mu\text{m}$ . The outer diameter of the tubes varies a lot due to the different number of clay layers which are rolled into the tubes. For the composites, although the coating layers seem to be uniform and cover the entire surface of the halloysites, many protuberance and small pores appear on the tube surfaces in the highly magnified images (Fig. 4c, d), which can be contrasted with the smooth surfaces of the pristine clay nanotubes (Fig. 4a, b). The thickness of the uneven polymer coating is less than 15 nm and the diameter of most pores is less than 30 nm (Fig. 4c, d). The nanopores appear like white spots in SEM image (Fig. 4e). The porous structure of the composite was also characterized by nitrogen adsorption–desorption measurement. The results indicated that the sample had Barret–Jovner–Halenda pore volume of  $0.06 \text{ cm}^3/\text{g}$ , and a maximum pore size distribution of about 32 nm, which is in accordance with the microscopic observations. It is noted that although polymer-coated halloysite tubes prepared with the solution-based method have been reported recently [23, 24], the microstructure of such multi-pored polymer-coated clay tubes has never been clarified so far.

To study the detailed microstructure of the composites, two further control experiments were done. After removing the polymer shell with *N*-methylpyrrolidone, the clay

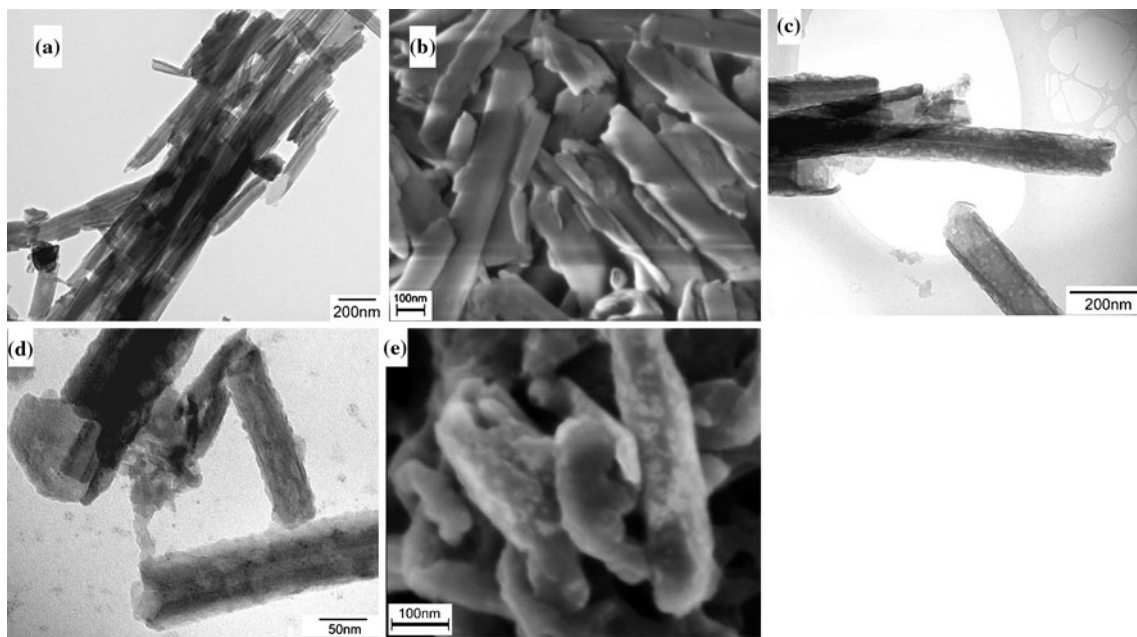


**Fig. 4** TEM image of **a** halloysites and **c, d** PANi/halloysite composite; SEM image of **b** halloysites and **e** PANi/halloysite composite

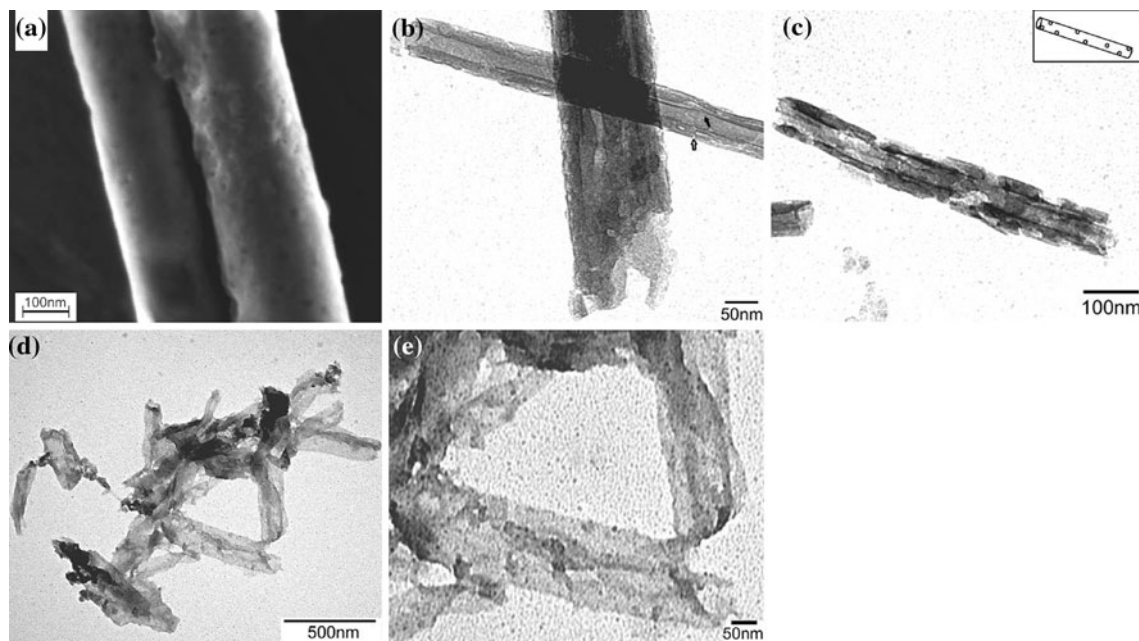


**Fig. 5** TEM (a, b) and SEM (c) image of halloysites tubes after removal of PANi outerlayer and TEM (d, e) images of PANi nanotubes after removal of clay cores

exhibits multi-holed tube structure (Fig. 5a–c), however; the holes here are so different from those in Fig. 3d–f that most holes are indeed small black holes in SEM image (<15 nm), more irregular and vary a lot in size (Fig. 5b, c). It is revealing to study the penetration depth of the holes in the multi-walled clay tube. As shown in Fig. 5b, c, some holes are through the tubewalls. The solid arrow in Fig. 4b shows the enlarged inner tube diameter due to the holes making the wall compressed and curved, while the hollow arrow shows a hole just on the surface of the wall without penetrating it. The cartoon of a flute-like tube in Fig. 4c illustrates such a structure. Due to the multi-holed nanostructure, such novel clay nanotubes are expected to have improved properties compared to those without holes on the walls when using as adsorbents, substrates for catalysts, and nanocontainers for delivery microsystems. Further work on this material is underway. In contrast, after dissolving the clay cores with HCl–HF mixing acid, the remaining polymer shells show tube-like appearance (Fig. 5d, e). Due to their thin tubewalls, the PANi tubes cannot retain their tubular shape and shrink to smooth belts, which are different from those obtained with solution method [1, 25].

At present, the mechanochemical reaction mechanism involved in the process remains unclear. However, it is believed that the formation of the PANi and the nanoholes in the sidewall of the clay tubes is likely related to the mechanochemical polymerization process. At the beginning of the reaction, aniline is easily absorbed on the surfaces of the halloysite nanotubes through H-bond

interaction. When mixing with  $\text{FeCl}_3$ , both the Lewis base characteristic of aniline and the strong Lewis acid characteristic of  $\text{FeCl}_3$  benefit the reaction between them [26]. Mechanical grinding not only causes new  $\text{FeCl}_3$  surfaces for further reaction with aniline but also improves the interfacial diffusion between the reactants and halloysite. As the diffusion of the solid reactant particles is often short-range during the mechanochemical reaction, thus it helps to restrict the polymerization in a limited area on the surfaces of the clay tubes. The continually released HCl by-product from the polymerization benefits not only the auto-catalyzing polymerization of PANi on the surfaces of clay tubes but also in situ etching of the clay tube walls, resulting in many small holes (Fig. 5a–c).

## Conclusion

A facile mechanochemical polymerization process for synthesis of multi-pored PANi nanolayer modified halloysite nanotubes with holes in the tubewalls was developed. Microscopic examinations confirmed the presence of nanoholes on the clay tube walls and porous PANi nanolayer coatings. Moreover, PANi nanotubes and multi-holed clay nanotubes can be obtained by further chemical treatment of the composite.

**Acknowledgements** The authors are grateful for access to the characterization facilities in the Australian Microscopy & Microanalysis Research Facility at the Australian Centre for Microscopy and Microanalysis, University of Sydney. C.Z. acknowledges the award of

an APA scholarship. Z.L. and X.D. would like to thank the Australian Research Council for the financial support.

## References

1. Hatchett DW, Josowicz M (2008) *Chem Rev* 108:746
2. Plesu N, Ilia G, Sfirloaga P, Iliescu S (2009) *J Mater Sci* 44:6437. doi:[10.1007/s10853-009-3895-8](https://doi.org/10.1007/s10853-009-3895-8)
3. Shi BF, Ren JW, Wang AM, Liu XH, Wang YQ (2009) *J Mater Sci* 44:6498. doi:[10.1007/s10853-009-3614-5](https://doi.org/10.1007/s10853-009-3614-5)
4. Kong LB, Zhang J, An JJ, Luo YC, Kang L (2009) *J Mater Sci* 43:3664. doi:[10.1007/s10853-008-2586-1](https://doi.org/10.1007/s10853-008-2586-1)
5. Chang QF, Zhao K, Chen X, Li MQ, Liu JH (2008) *J Mater Sci* 43:5861. doi:[10.1007/s10853-008-2827-3](https://doi.org/10.1007/s10853-008-2827-3)
6. Ding Y, Tursun A, An S, Ismayil N (2008) *J Appl Polym Sci* 107:3864
7. Šeděnková I, Trchová M, Stejskal J, Prokeš J (2009) *ACS Appl Mater Interface* 1:1906
8. Du XS, Zhou CF, Wang GT, Mai Y-W (2008) *Chem Mater* 20:3806
9. Tursun A, Zhang XG, Ruxangul J (2005) *Mater Chem Phys* 90:367
10. Zhao MF, Liu P (2008) *Microporous Mesoporous Mater* 112:419
11. Ning NY, Yin QJ, Luo F, Zhang Q, Du R, Fu Q (2007) *Polymer* 48:7374
12. Machado GS, Castro K, Wypych F, Nakagaki S (2008) *J Mol Catal A* 283:99
13. Shamsi MH, Geckeler KE (2008) *Nanotechnology* 19:075604
14. Joussein E, Petit S, Churchman J, Theng B, Righi D, Delvaux B (2005) *Clay Miner* 40:383
15. Belver C, Bañares Muñoz MA, Vicente MA (2002) *Chem Mater* 14:2033
16. Franco C, Paolo M (2002) *Eur Polym J* 38:1791
17. Wu C-S, Huang Y-J, Hsieh T-H, Huang P-T, Hsieh B-Z, Han Y-K, HO K-S (2008) *J Polym Sci A* 46:1800
18. Karim MR, Yeum JH (2008) *J Polym Sci B* 46:2279
19. Zheng W, Angelopoulos M, Epstein AJ, MacDiarmid AG (1997) *Macromolecules* 30:7634
20. Liu DF, Du XS, Meng YZ (2006) *Mater Lett* 60:1847
21. Zhang L, Wang T, Liu P (2008) *Appl Surf Sci* 255:2091
22. Travas-Sejdic J, Soman R, Peng H (2006) *Thin Solid Films* 497:96
23. Zhang L, Liu P (2008) *Nanoscale Res Lett* 3:299
24. Li C, Liu J, Qu X, Yang Z (2009) *J Appl Polym Sci* 112:2647
25. Gao Y, Li X, Gong J, Fan B, Su Z, Qu L (2008) *J Phys Chem C* 112:8215
26. Niemi VM, Knuutila P, Österholm J-E, Korvola J (1992) *Polymer* 33:1559